The International Journal of Engineering and Science (IJES)
|| Volume || 11 || Issue || 9 || September || Pages || PP 30-49 || 2022 ||
ISSN (e): 2319-1813 ISSN (p): 20-24-1805

Numerical simulation of flow around three tandem cylinders

Bo-Jie Xu[1], Fei Wu[2], Ya-Peng Li[1], Hao-Chen[1], Li-Xin Chen[1], Qi-Kai Gong[1], Yin-Peng Li[1], Hong-Bin Sun[1]

1. College of Mechanical Engineering, Quzhou University, Quzhou, 324000, China;
2. Zhejiang Testing&Inspection Institute for Mechanical and Electrical Products Quality Co.,Ltd

ABSTRACT

The laminar flow model is used to simulate the two-dimensional, constant flow field of three tandem cylinders, focusing on the effect of different cylinder diameters and spacings on the structure and characteristics of the flow field. It is found that under the condition of Re=50, periodic vortices with stable shedding occur in the tail flow field of the cylinder. The increase of the distance between the cylinders will cause the extension of the length of the upstream tail flow field and the growth of the drag coefficient of the cylinders at both ends of the distance, and the increase of the diameter of the cylinders will rise the area of the tail flow field and its drag coefficient while reducing the drag coefficient of the downstream cylinders. The expansion limit value of the reflux zone is positively correlated with the upstream cylinder diameter, and the expansion degree is positively correlated with the spacing and negatively correlated with the downstream cylinder diameter. When the reflux zone is expanded to the limit, complete vortex shedding is formed in the tail flow field.

Keywords*: three tandem cylinders, diameter, spacing, constant, reflux zone*

Date of Submission: 27-09-2022 Date of Acceptance: 11-10-2022

I. INTRODUCTION

As a classical problem in fluid mechanics, flow around an obtuse body exists widely in daily life and practical engineering, such as water flowing over bridge piers, the wind blowing over tall towers, oil pipelines in the ocean, etc. At the beginning of the twentieth century, Theodore von Karman discovered in his experiments that under certain conditions, two alternating vortex structures with opposite rotational directions would be formed at the tail flow field of the cylinder. After an in-depth understanding of this phenomenon, he proposed the famous "Karman vortex street" theory.

Prandtl et al. proposed that the fluid passing through the cylinder can be divided according to the flow characteristics into a boundary layer zone near the surface of the cylinder, which is mainly subject to fluid viscous friction, and a mainstream zone nearby, where the viscous friction is less. When the fluid flows through the cylinder structure, the area of the overflow close section decreases along the course, the flow velocity gradually increases and the pressure gradually decreases[1].

In the presence of a negative pressure gradient, due to the effect of fluid viscosity, fluid microelements in the mainstream zone with higher energy can continue to move forward, while fluid microelements in the boundary layer with lower energy will be subject to strong resistance and decelerate, and the velocity decreases to 0 and then moves in reverse. This part of the fluid is more and more, the formation of the reflux zone to expand outward, the mainstream zone flow separation, and the formation of a separate shear layer on the surface of the cylinder. The tail of the shear layer will form alternating, periodic shedding vortices under certain Reynolds number conditions, also known as Karman vortex street. The vortex will produce a periodic force on the cylinder, which can be decomposed into a component force along the direction of flow and perpendicular to the direction of flow, the former is called drag and the latter is called lift[2].

Liu Shan et al. [3]simulated the flow field characteristics around a double-pile foundation under the action of unidirectional flow by constructing a three-dimensional numerical flume to analyze the effects of different spacings and different head-on angles on the flow field structure around the pile. Gu Gang[4] explored the two-dimensional non-constant flow around solid cylinders in a laminar flow state, and analyzed the change of the value of the lift and drag coefficients, the motion and shedding of the vortex in the flow field by using the finite volume method and SIMPLE algorithm under FLUENT software and verified the validity of the numerical solution to the problem. Du Xiaoqing et al. [5], to explore the internal variation of the characteristics

of the flow field around tandem double cylinders with different spacings, performed the modal decomposition of the flow field of tandem double cylinders with spacing ratios of P/D=1.1~5 at *Re*=100 by the kinetic modal decomposition method and reconstructed the vortex field of tandem double cylinders with establishing a reduced-order model based on the dominant modal of DMD. Jiang Ke et al. [6]conducted a two-dimensional numerical simulation of cylindrical winding flow at subcritical Reynolds number, based on which a simulation analysis of deep-water riser winding flow containing an additional rod was carried out, and the outstanding effect of the additional rod in suppressing the riser cylindrical winding flow was confirmed.

Chen Suqin et al. [7] used an improved MAC method with multiple grids in a third-order upwind format for the convective item to simulate the flow field of two parallel square columns to study their aerodynamic and mutual interference. Wang and Tan[8] investigated the structure of the wake flow field behind the cylindrical and square columns near the flat plate. Tong Xiaojian [9] simulated and analyzed the flow field characteristics of equal-diameter parallel double-cylinder and triple-cylinder winding flow at different spacing ratios using FLUENT software. Yin Jianjun et al. [10] conducted a numerical simulation study on seven-array cylinders in the form of isometric staggered arrangement and nine-array cylinders in the form of isometric square quadrilateral arrangement and found that the change of wake structure is closely related to the transition of wake pattern.

This paper intends to solve the problem of two-dimensional constant flow around three tandem cylinders in laminar flow with low Reynolds number *Re*=50 by FLUENT software, to numerically simulate the flow field around three tandem cylinders with different diameters and spacings, to obtain the velocity change, flow line, pressure distribution, vorticity distribution and changes in drag coefficients of the flow field, and to analyze the influence of the cylindrical diameter and spacing on the structure and characteristics of the flow field around three tandem cylinders by these results and data.

II. NUMERICAL SIMULATION METHODS

2.1 Computational Model

Figure 1 shows the computational model of the flow around three tandem cylinders. The inlet is 10*D* from the center of the upstream-most cylinder and the outlet is 280*D* from the center of the upstream-most cylinder. The diameter of the cylinders is D_1, D_2, D_3, the spacing is L_1, L_2, and the speed of incoming flow U=0.031m/s. We use D_1, D_2, D_3, L_1, L_2, and L=L_1=L_2 as six variables, and then divide six groups of parameters with unique variables. In each group of parameters, we use the control variable method to study the effect of a single variable on the flow field around three tandem cylinders, including the variation law of velocity, vorticity, pressure, drag coefficient, and other characteristics.

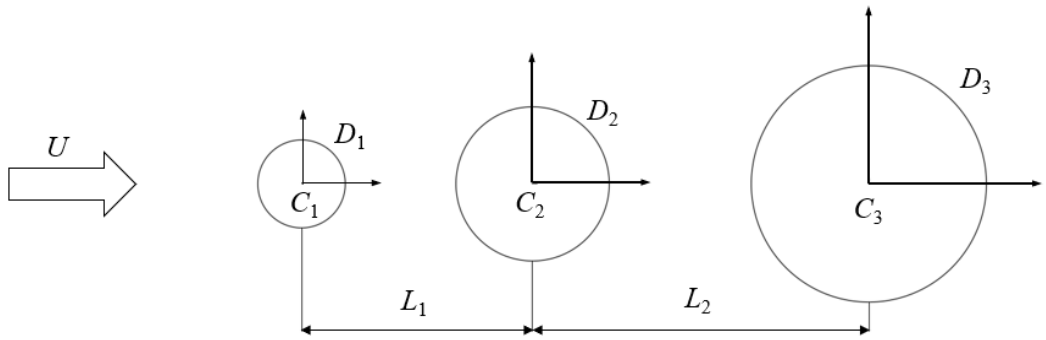

Figure 1 computational model

This paper intends to numerically simulate the two-dimensional, incompressible flow field around three tandem cylinders under the condition of *Re*=50. The model parameters of the flow field are shown in Table 1.

Table 1 Two-dimensional model parameters description (*D*=10mm)

Number	D_1/D	D_2/D	D_3/D	L_1/D	L_2/D
1	1	2	3	3,4,5,6,7	4
2	1	2	3	4	3,5,6,7,8
3	1	2	3	5,6,7,8,9	5,6,7,8,9

4	1.2,1.4,1.6,1.8,2	2	3	8	8
5	1	2.2,2.4,2.6,2.8,3	3	8	8
6	1	2	3.2,3.4,3.6,3.8,4	8	8

2.2 Grid division

ICEM software is used to divide the mesh of the 2D model, and the global calculation domain is a rectangle of 0.1m×2.8m. The computational model uses unstructured grids, and the total number of grids in the computational domain is 33056. The grid encryption zone is set up in the area near the three cylinders, and a boundary layer grid is set up on the wall of the cylinders with a minimum height of 0.5mm, a growth rate of 1.25, and the number of layers is 5~7. After checking, the overall quality of the grid is greater than 0.4, which meets the calculation requirements of the tail flow field and boundary layer. Figure 1 shows the grid division of the computational domain.

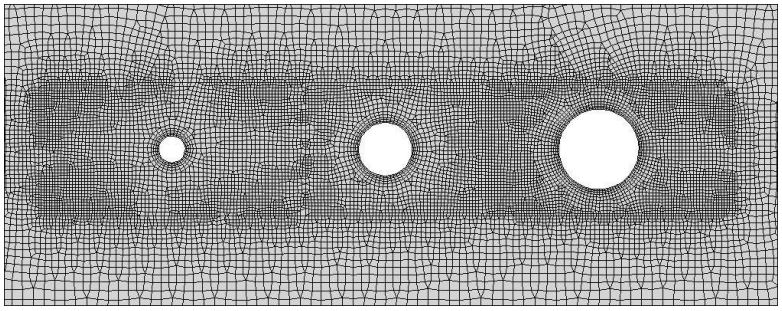

Figure 2 Partial grid

2.3 Solution controls

In this paper, the laminar flow model in the commercial software FLUENT is used to numerically simulate the flow field around three tandem cylinders at *Re*=50. For this two-dimensional flow problem, the fluid is considered as a viscous incompressible fluid. The continuity equation and momentum equation (N-S equation) in the oxy right-angle coordinate system are[5]:

$$\frac{\partial u}{\partial x}+\frac{\partial v}{\partial y}=0 \tag{1}$$

$$\rho\frac{Du}{Dt}=\rho F_x-\frac{\partial p}{\partial x}+\mu\left(\frac{\partial^2 u}{\partial x^2}+\frac{\partial^2 u}{\partial y^2}\right) \tag{2}$$

$$\rho\frac{Dv}{Dt}=\rho F_y-\frac{\partial p}{\partial y}+\mu\left(\frac{\partial^2 v}{\partial x^2}+\frac{\partial^2 v}{\partial y^2}\right) \tag{3}$$

Where ρ is the fluid density, p is the fluid pressure, μ is the viscosity coefficient, u and v are the velocity components in the *x* and *y* directions respectively, F_x and F_y are the body forces of the fluid in the *x* and *y* directions respectively.

Using air as the flow medium, fluid density ρ = 1.225 kg·m^{-3}, kinetic viscosity μ = 1.789×10^{-5}N·s·m^{-2}. Since the adopted Reynolds number *Re*=50 belongs to the low-velocity laminar flow state, the laminar flow model is chosen.

The numerical simulation uses a rectangular calculation domain, and the inlet uses velocity inlet boundary conditions. Free outflow boundary conditions are used for the outflow. The cylindrical wall surface uses a no-slip wall condition. Symmetric surface boundary conditions are used for the upper and lower walls of the far field.

In this paper, the pressure-based solver in FLUENT software, which is suitable for the flow characteristics of low-velocity incompressible flow, is used to simulate the fluid flow. The gradient algorithm uses cell-based least squares difference. The spatial discretization of the convective item is in second-order

windward format. The coupling of speed and pressure is implemented using the SIMPLE algorithm. The default under-relaxation factor is used for all variables in the iterative calculation, and the residual convergence accuracy is 1e-6.

III. ANALYSIS OF RESULTS

3.1 Velocity field

To study the flow field characteristics and the variation law of the flow around three tandem cylinders under different cylindrical spacing and diameter conditions, we display and superimpose the velocity cloud maps and average flow line diagrams for six groups of parameters.

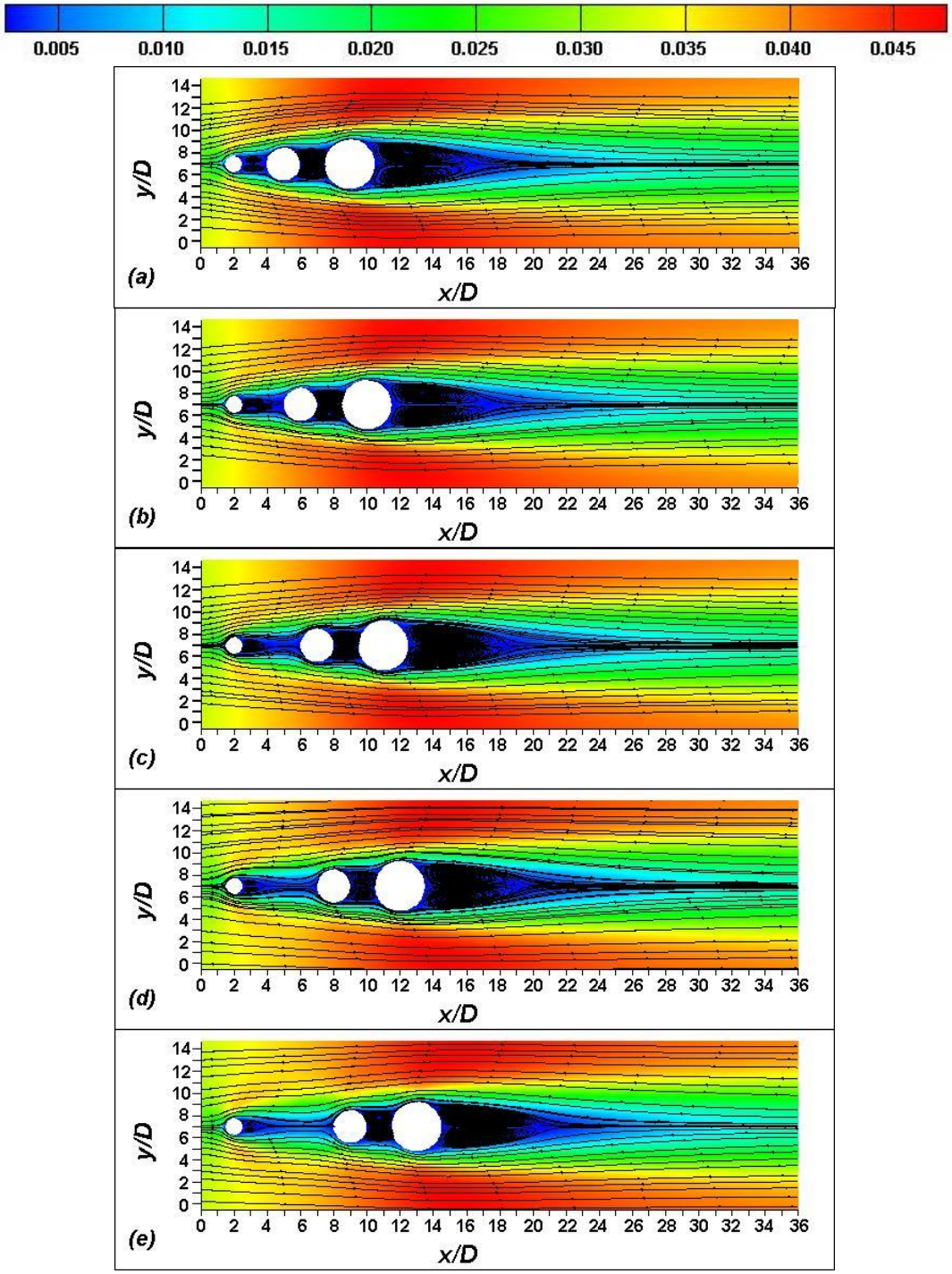

Figure 3 Velocity cloud map (*a*)L_1/D=3,(*b*)L_1/D=4,(*c*)L_1/D=5,(*d*)L_1/D=6,(*e*)L_1/D=7

As shown in Fig. 3, at L_1/D = 3, the expansion of the reflux zone of upstream cylinder C_1 and midstream cylinder C_2 is obstructed by the wall surface of the rear cylinder. At L_1/D = 4, 5, 6, 7, the reflux zone of upstream cylinder C_1 expands to the limit, a stable vortex shedding is formed in the tail flow field, and the vortex in the tail flow field of downstream cylinder C_3 shifts to the right with the rightward shift of the cylinder position. By comparing the tail of the flow field of the upstream cylinder and the downstream cylinder, it can be found that when the spacing L_1 increases, the reflux zone expands to a certain degree and then no longer changes, while the width of the low-velocity area gradually decreases along the course and finally converges to a point. By comparing the variation of the upstream cylindrical and midstream cylindrical tail flow field, it is concluded that when the spacing between the cylinders is less than the limit value, the downstream cylindrical wall will play a suppressive role in the expansion of the upstream cylindrical tail flow field and the formation of complete vortex shedding.

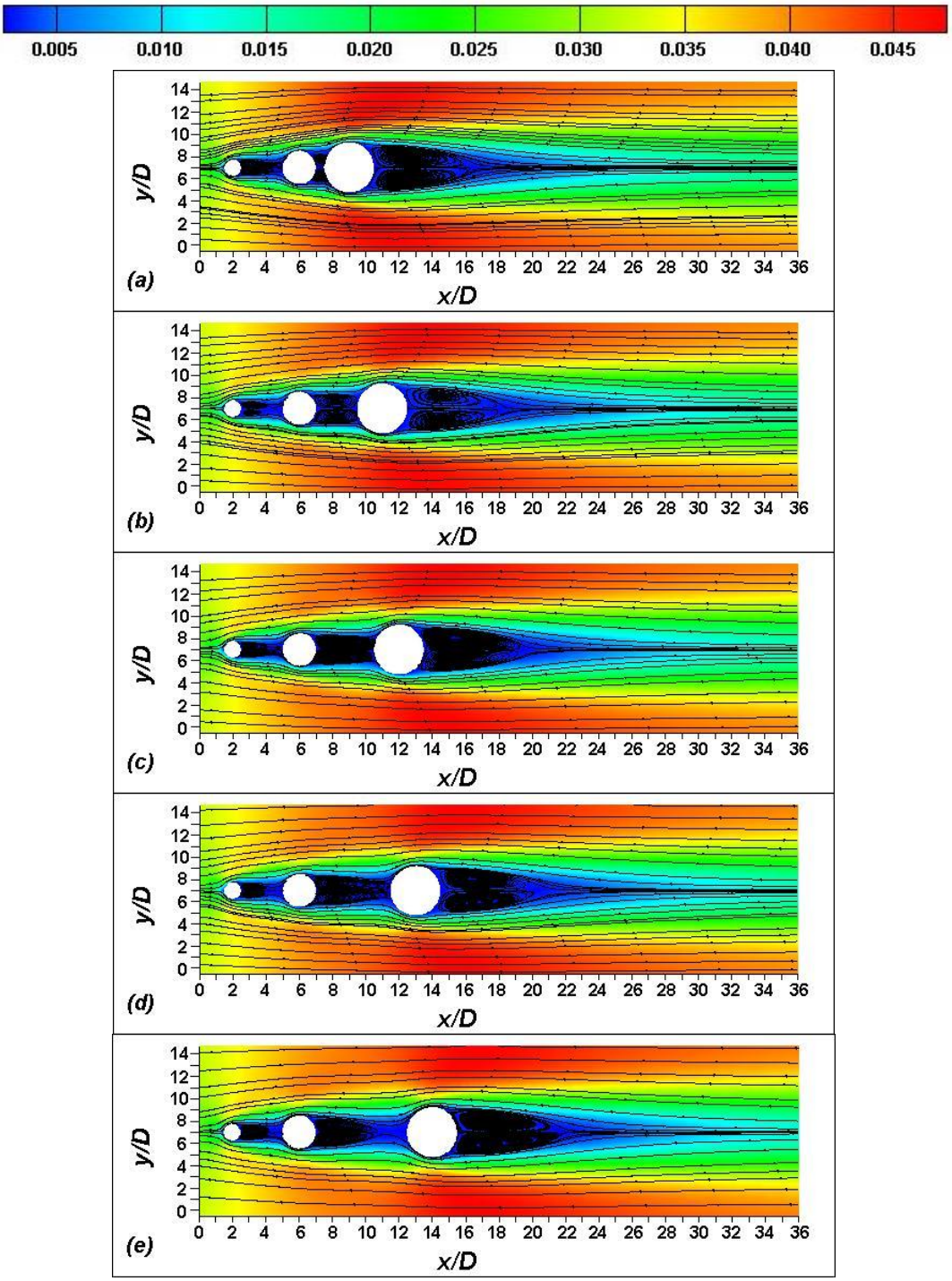

Figure 4 Velocity cloud map (*a*)L_2/D=3,(*b*)L_2/D=5,(*c*)L_2/D=6,(*d*)L_2/D=7,(*e*)L_2/D=8

As seen in Figure 4, when the spacing L_2 between the midstream cylinder C_2 and the downstream cylinder C_3 increases, the reflux zone of C_2 continuously expands outward. At L_2/D=8, the reflux zone of C_2 stops expanding, and the complete vortex shedding motion is formed in the tail flow area at this time. It can be found that when the cylinder spacing is less than the limit value, the downstream cylinder wall surface inhibits the formation of complete vortex shedding in the wake of the upstream cylinder, and the size of the spacing limit value is positively related to the diameter of the upstream cylinder. There is no significant change in the shape and structure of the tail flow field of upstream cylinder C_1, and the position of the tail flow field of downstream cylinder C_3 shifts to the right with the increase of spacing L_2, which leads to the conclusion that in the flow field around three tandem cylinders, the change of cylinder spacing does not affect flow field of the upstream non-adjacent cylinder.

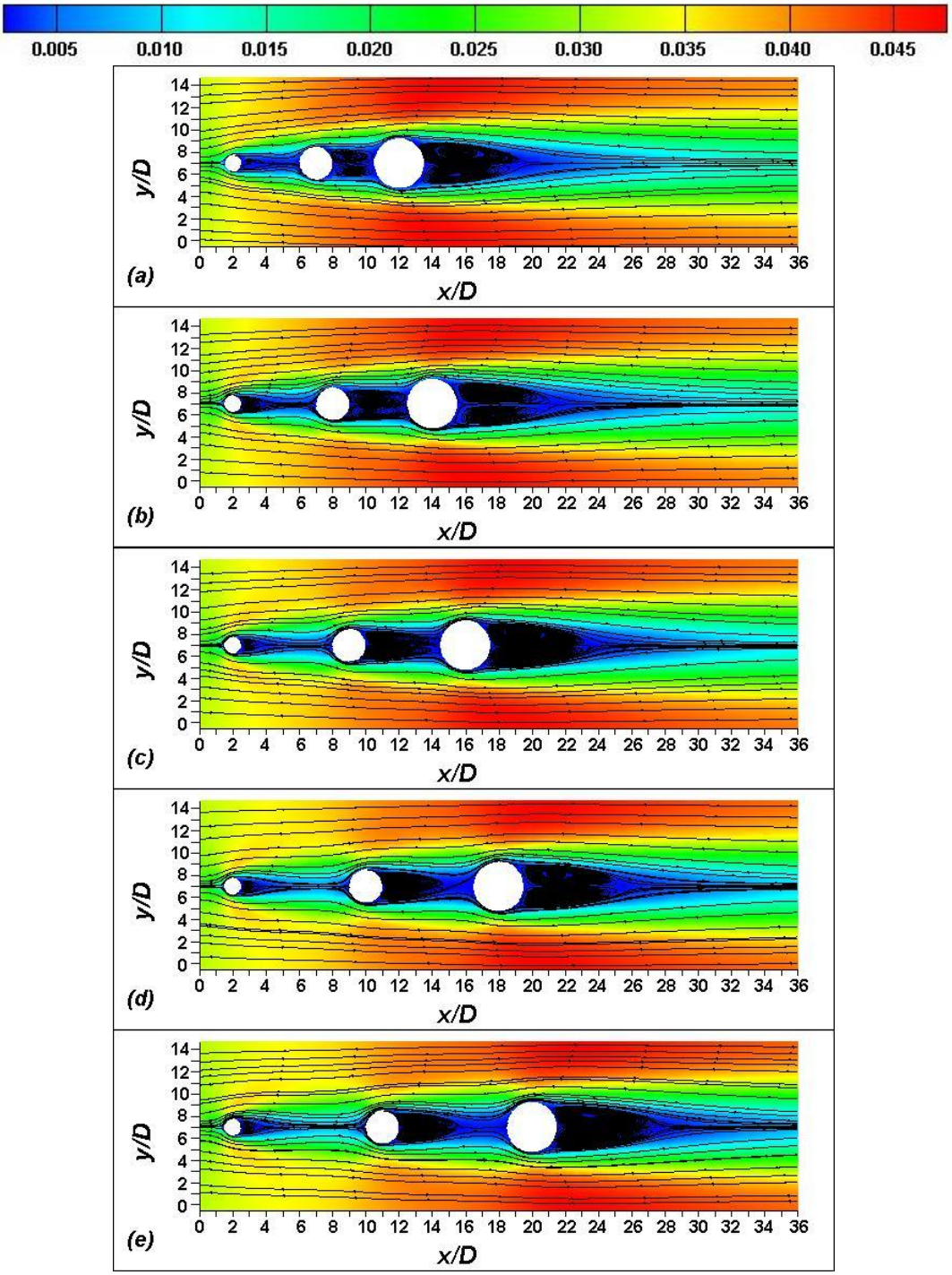

Figure 5 Velocity cloud map (L=L_1=L_2) (*a*)L/D=5,(*b*)L/D=6,(*c*)L/D=7,(*d*)L/D=8,(*e*)L/D=9

To further analyze the effect of the cylindrical spacing on the flow field, as shown in Figure 5, we compare L_1 and L_2 as variable L. It can be observed from Figs. (*d*) and (*e*) that when L/D = 8 and 9, all three cylindrical tail reflux zone stop expanding outward and the tail flow area produces a complete vortex shedding motion. It can be concluded that when the cylinder spacing exceeds a limit value, the increase in spacing does not affect the zone of the upstream cylinder with vortex shedding. And when the cylindrical spacing is less than the limit value, the upstream neighboring cylindrical tail flow area cannot produce complete vortex shedding motion, and as the cylindrical spacing increases, the reflux zone of the upstream cylinder continues to expand outward.

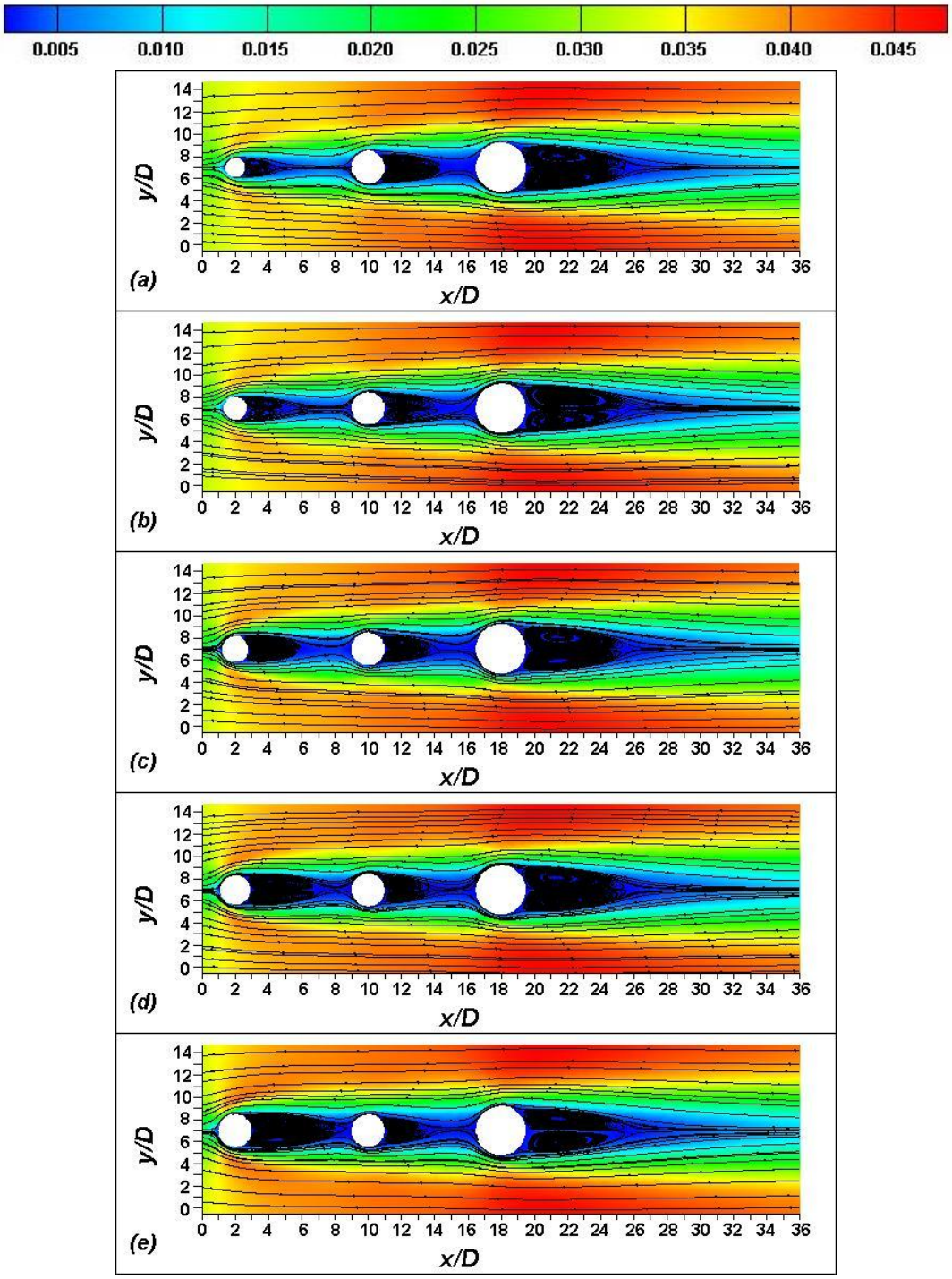

Figure 6 Velocity cloud map (*a*)D_1/D=1.2,(*b*)D_1/D=1.4,(*c*)D_1/D=1.6,(*d*)D_1/D=1.8,(*e*)D_1/D=2

As shown in Figure 6, when D_1/D=1.2, the center of the reflux zone of the upstream cylinder C_1 lies on the straight line x/D=3.5, and the center of the reflux zone of the midstream cylindrical C_2 tail flow field is on the straight line x/D=12.5. When D_1/D=2, the position of the transverse coordinate of the center of the reflux zone of C_1 is near x/D=4.7; the transverse coordinate of the center of the reflux zone of C_2 is x/D=12. We compared the values and found that the vortex position in the upstream wake continued to shift in the downstream direction while the length and width of the reflux zone increased when the cylinder diameter D_1 continued to increase; in contrast, the vortex position in the tail flow field of C_2 continued to shift in the upstream direction while the length and width of the reflux zone decreased; the tail flow field of C_3 showed no significant change.

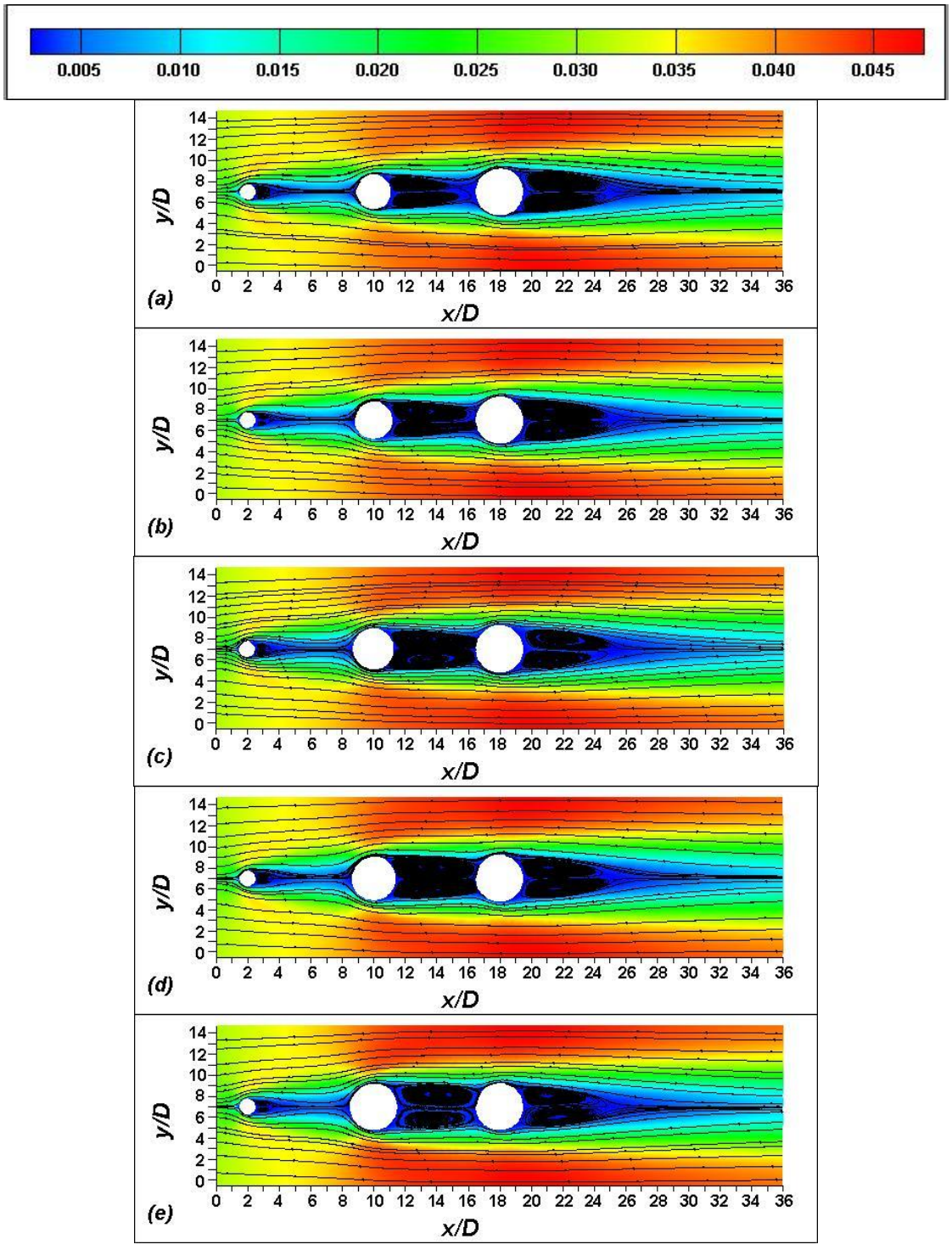

Figure 7 Velocity cloud map (*a*)D_2/D=2.2,(*b*)D_2/D=2.4,(*c*)D_2/D=2.6,(*d*)D_2/D=2.8,(*e*)D_2/D=3

As shown in Figure 7, the change in the cylindrical diameter of C_2 has no significant effect on the reflux zone of upstream cylinder C_1, but there is a small increment in the width of the part of its wake near the wall of C_2. In Figs. (*b*), (*c*), (*d*), and (*e*), the reflux zone of cylinder C_2 has not reached the maximum expansion, which means that the spacing L_2 does not satisfy the limit value at the current diameter, and no complete vortex shedding motion is formed in the tail flow area at this time; no significant changes are found in the tail flow area of downstream cylinder C_3. From the above observed, it can be tentatively concluded that the variation in the midstream cylindrical tail flow area does not cause significant effects on the downstream cylindrical tail flow area when the cylindrical spacing does not reach a limit value.

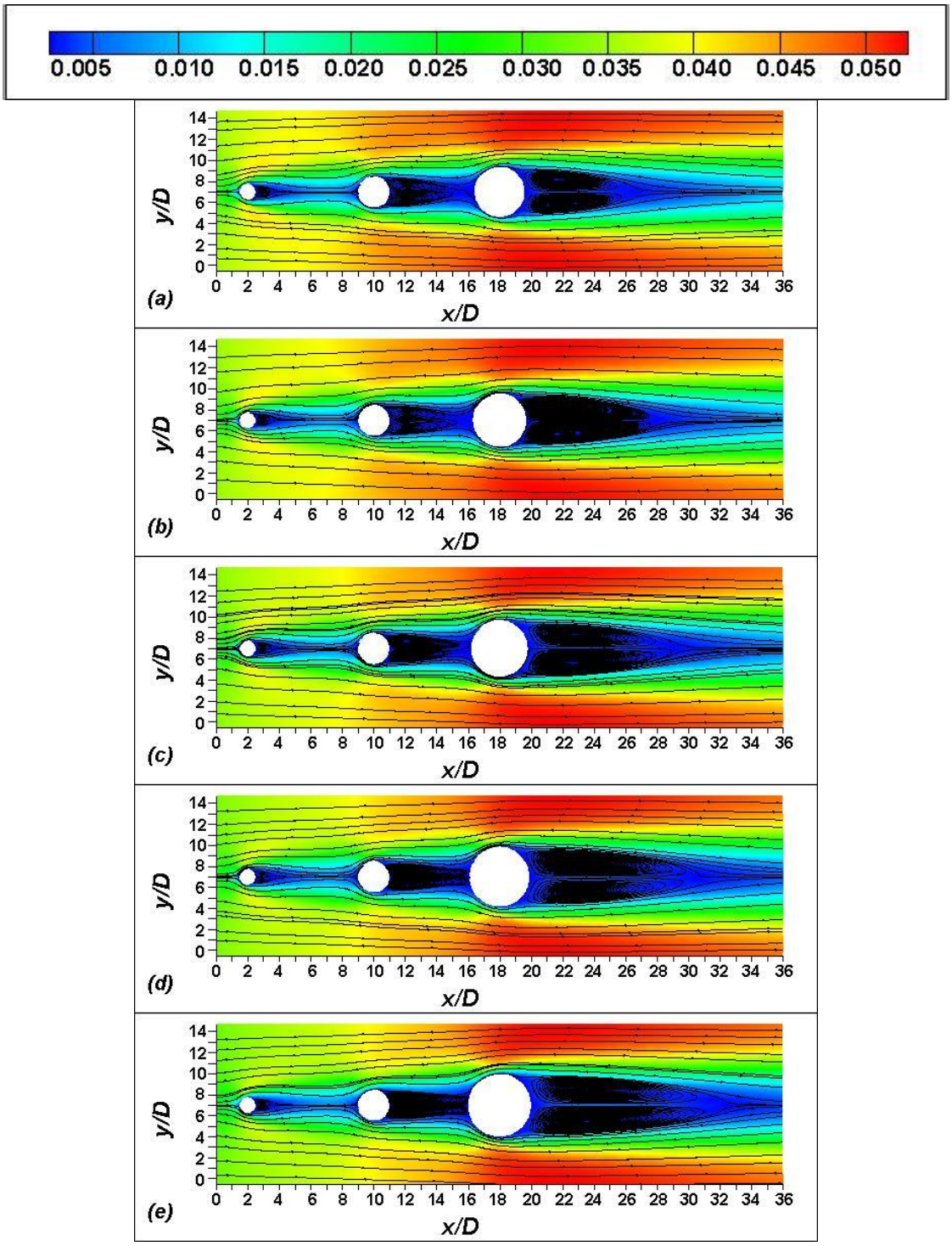

Figure 8 Velocity cloud map (*a*)D_3/D=3.2,(*b*)D_3/D=3.4,(*c*)D_3/D=3.6,(*d*)D_3/D=3.8,(*e*)D_3/D=4

As shown in Figure 8, when the diameter D_3 of the downstream cylinder C_3 increases, there is no significant change in the flow field around the cylinder and the tail flow field of C_1; the position of the center of the C_2 reflux zone on the transverse coordinate moves from near x/D=12.5 in Figure (*a*) to near x/D=13.5 in Figure (*e*); the location of the reflux zone in the C_3 tail flow field remains the same, but the width of the low-velocity tail flow area intercepted on the x/D=36 line in the figure increases significantly with the increase of D_3. Since the expansion of the reflux zone is essentially an increase of fluid microelements in the direction opposite to the main flow, the length of the reflux zone must also increase. Combining the effects of changes in the diameter and spacing of the three cylinders on the flow field around the three tandem cylinders' velocity field, we conclude that: When the cylinder diameter is fixed, there is a limit value of the spacing between two adjacent cylinders, and before reaching the limit value, the downstream cylindrical wall surface plays an inhibiting role in the expansion of the upstream cylindrical tail reflux zone, at which time the vortex shedding in the upstream cylindrical tail flow area is incomplete; after reaching the limit value, the spacing continues to increase, the reflux zone no longer changes, the complete vortex shedding motion is formed, the width of the low-speed tail flow area is reduced along the course, and finally converge into a point. When the cylindrical spacing is fixed, the size of the limit spacing between two adjacent cylinders is positively related to the diameter of the upstream cylinder, and the strength of the inhibitory effect of the wall surface of the downstream cylinder on the expansion of the reflux zone of the upstream cylinder is positively related to the diameter of the downstream cylinder.

3.2 Vorticity and pressure field

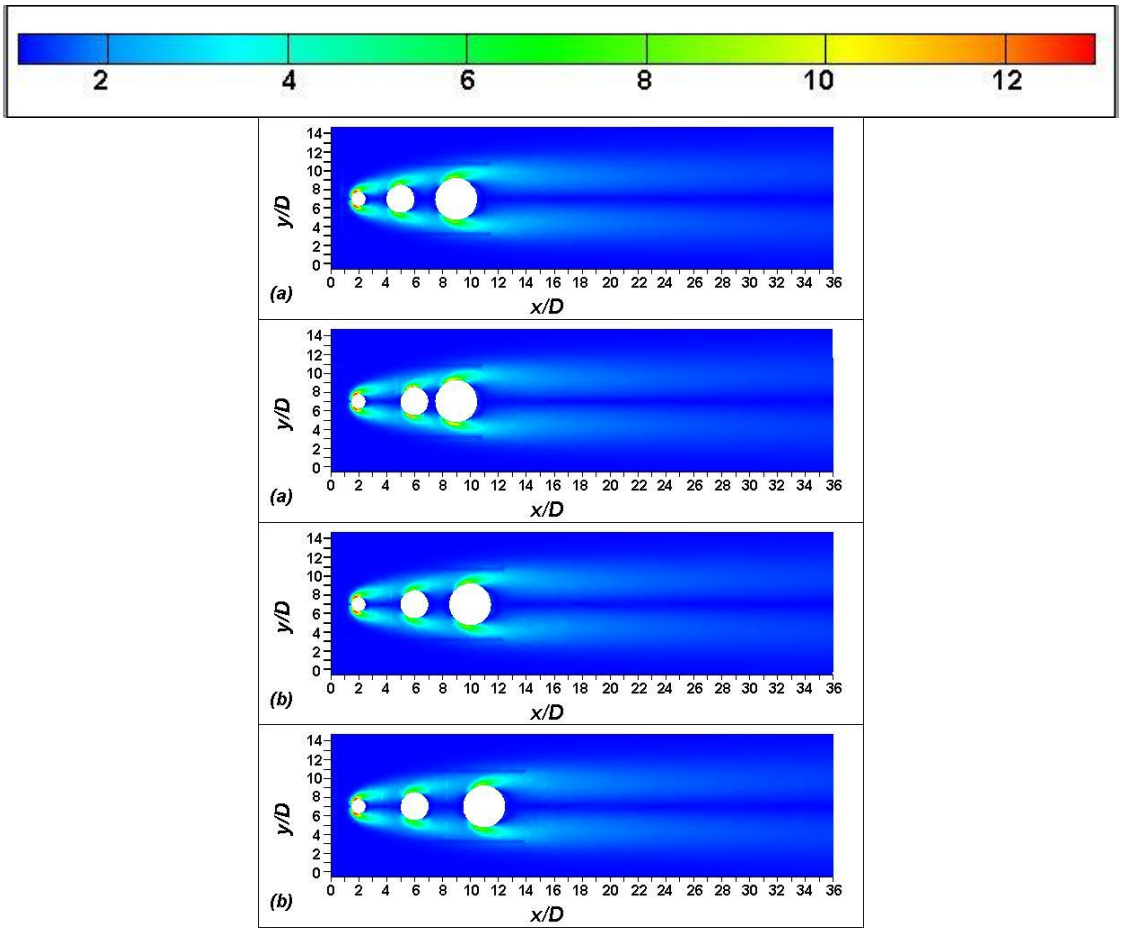

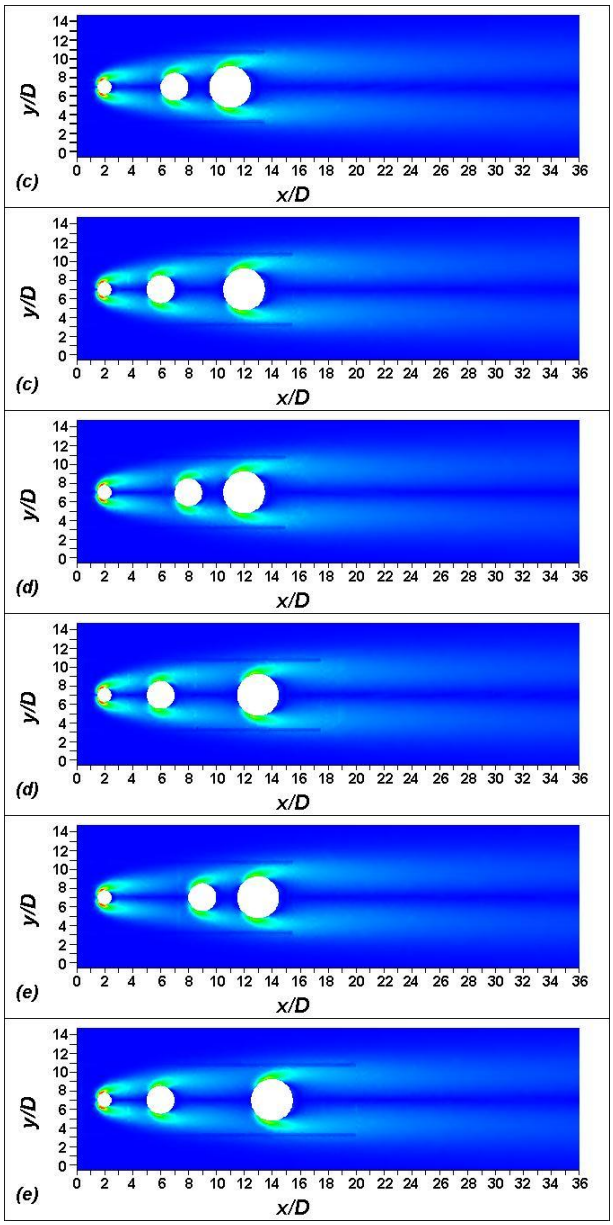

(1) (2)

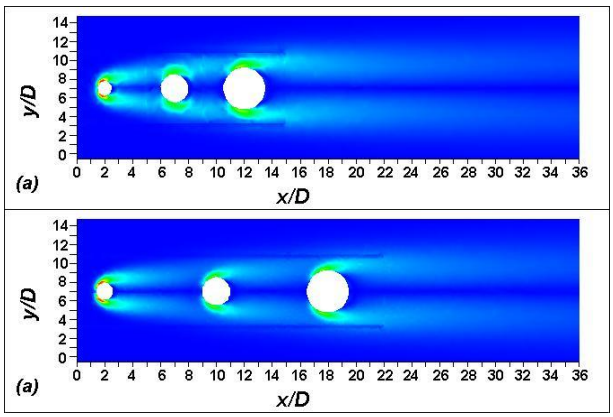

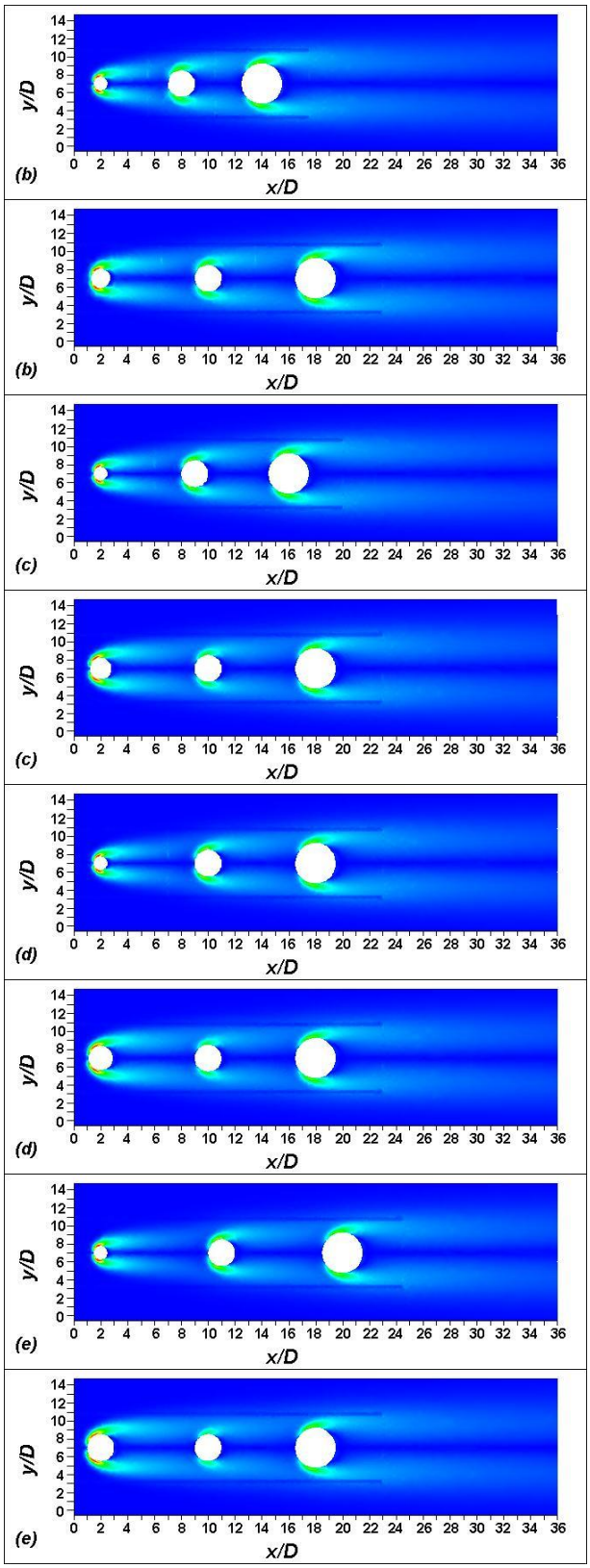

(3) (4)

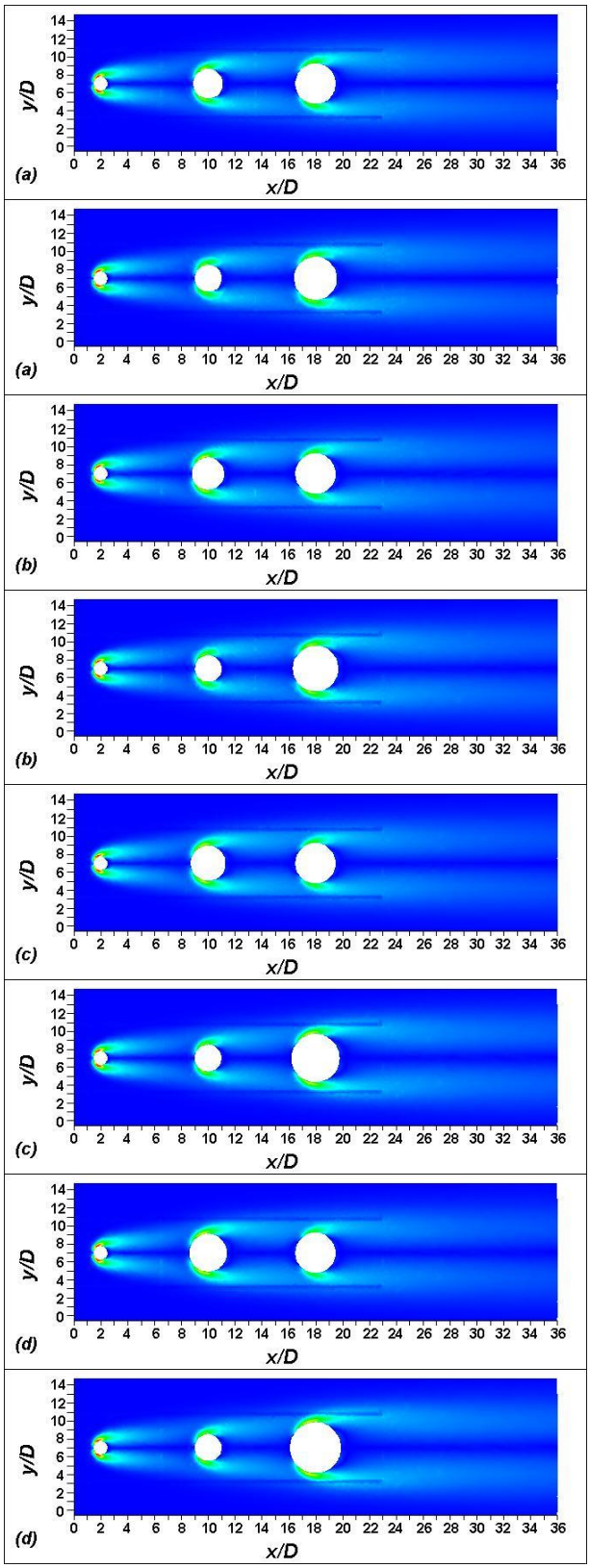
y/D
x/D
(a)
(a)
(b)
(b)
(c)
(c)
(d)
(d)

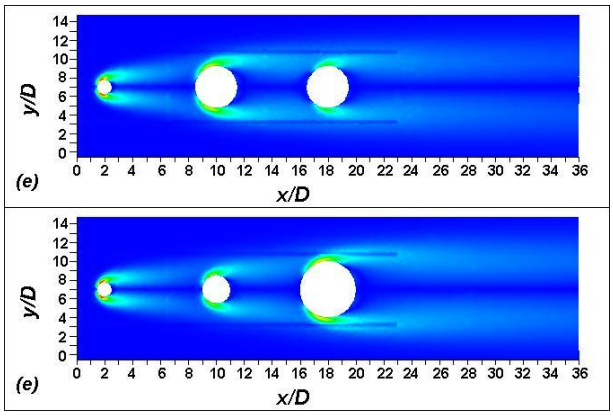

(5) (6)

Figure 9 vorticity cloud map

As shown in Figure 9, six sets of vorticity cloud maps of the three-cylinder flow field with different parameters are superimposed and compared, and it can be found that all six sets of cloud maps are symmetrically distributed with the line connecting the center of the three cylinders as the axis. The maximum vorticity is located in front of the side of the upstream cylinder C_1 facing the incoming flow, near the shear layer, and then gradually decays downstream along the cylindrical wall surface, with the shape spreading backward and outward from the crescent shape. The vorticity minimum is directly behind the cylinder and at other locations in the flow field. Among them, Figs. (1), (2), and (3) show the changes in the flow field vorticity when the spacing of the cylinders is varied, and it can be observed that two symmetric gradient ribbons exist on the outer side of the tail flow field of all three cylinders, and when the spacing is too small, the downstream cylindrical wall has an obstructive effect on the diffusion of the ribbon in the length and width directions. Figs (4), (5), and (6) show the variation of the flow field vorticity when the cylinder diameter is varied, and again it can be seen that the degree of diffusion of the ribbon is positively related to the cylinder diameter.

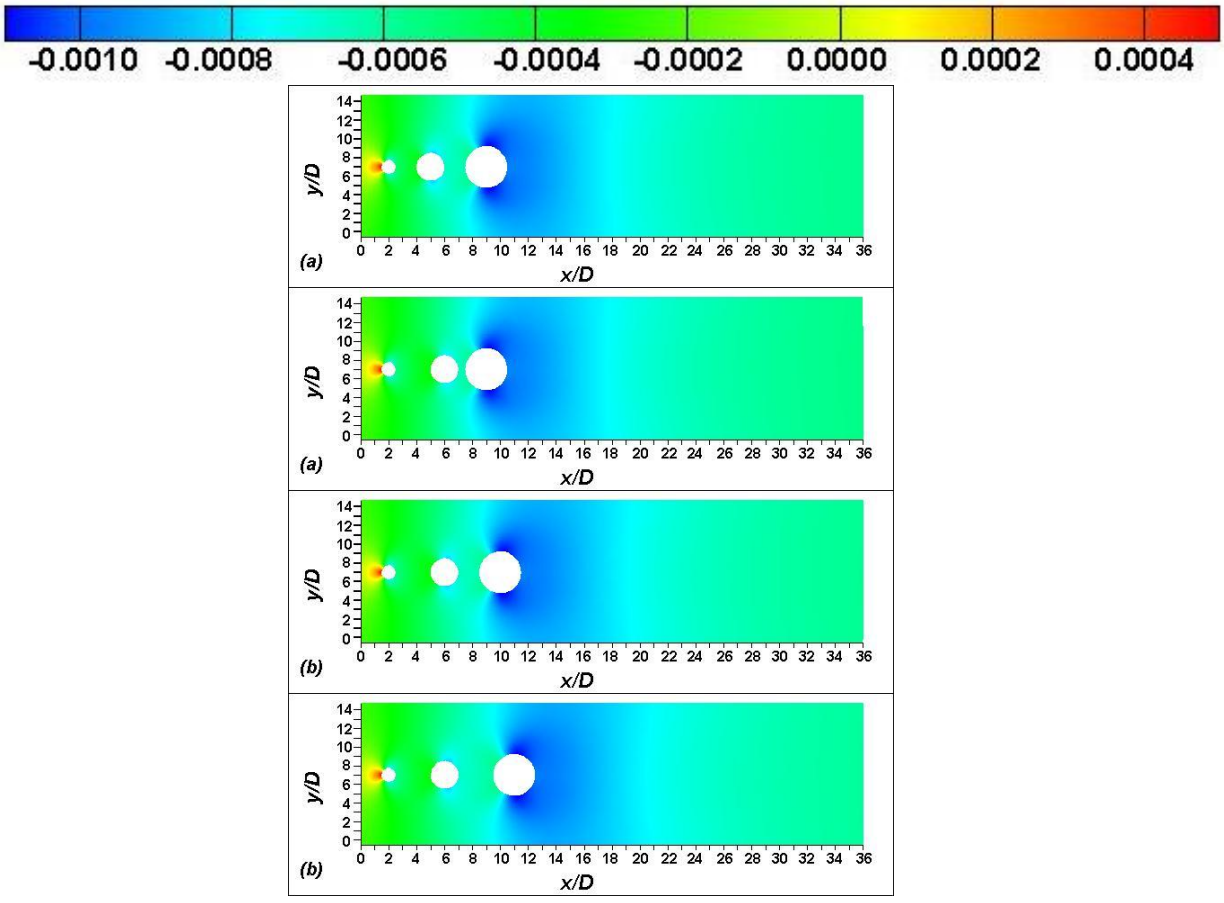

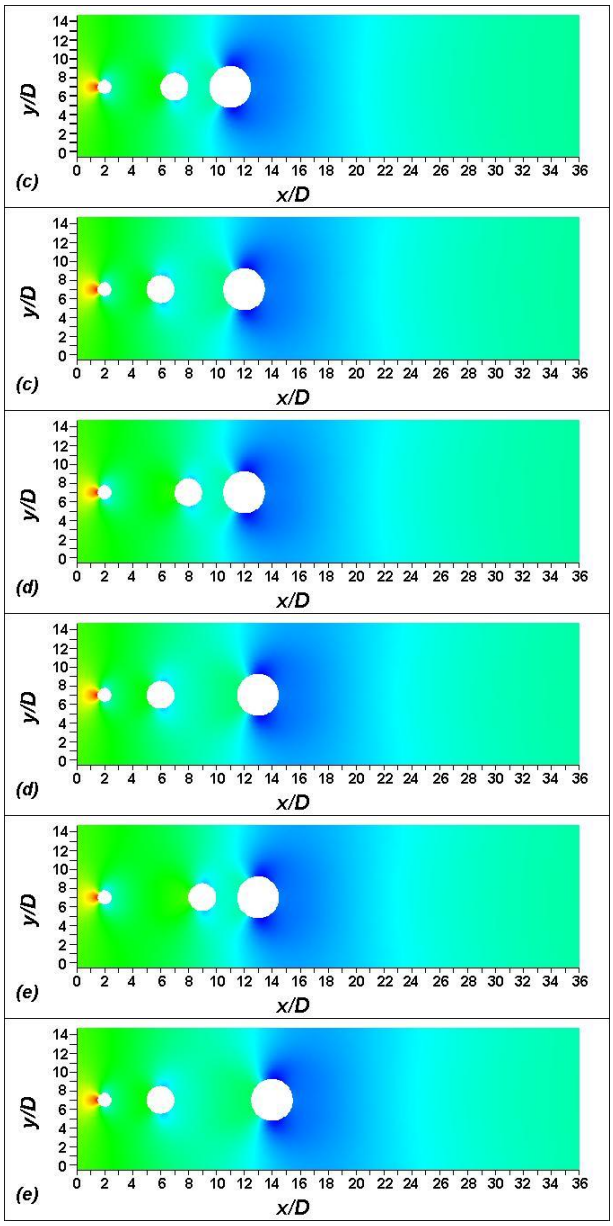

(1) (2)

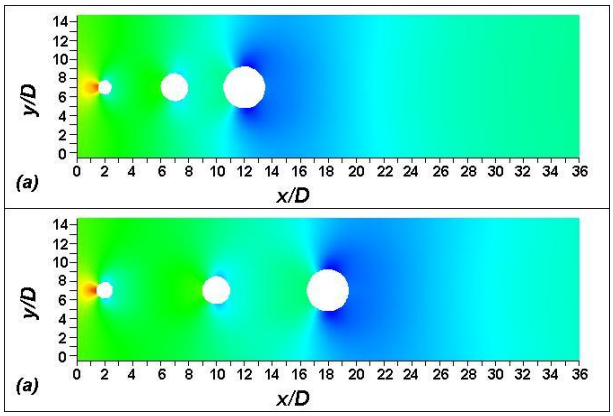

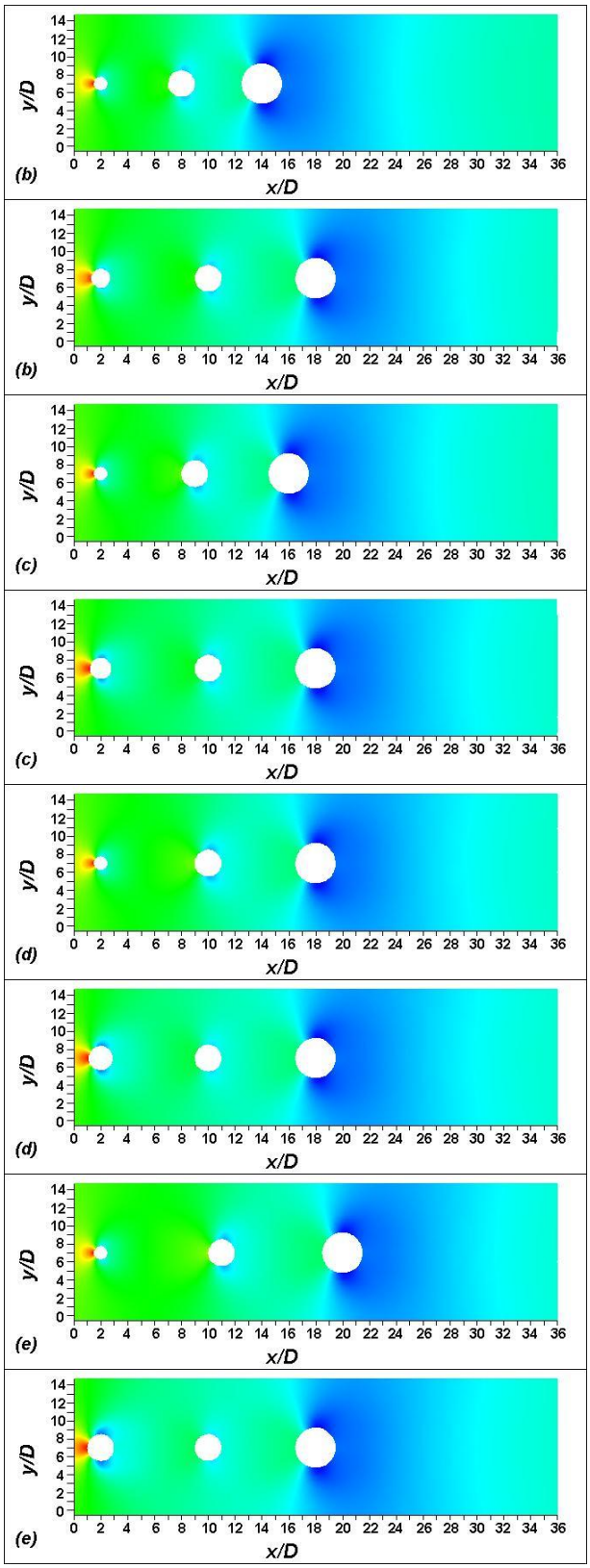

(3) (4)

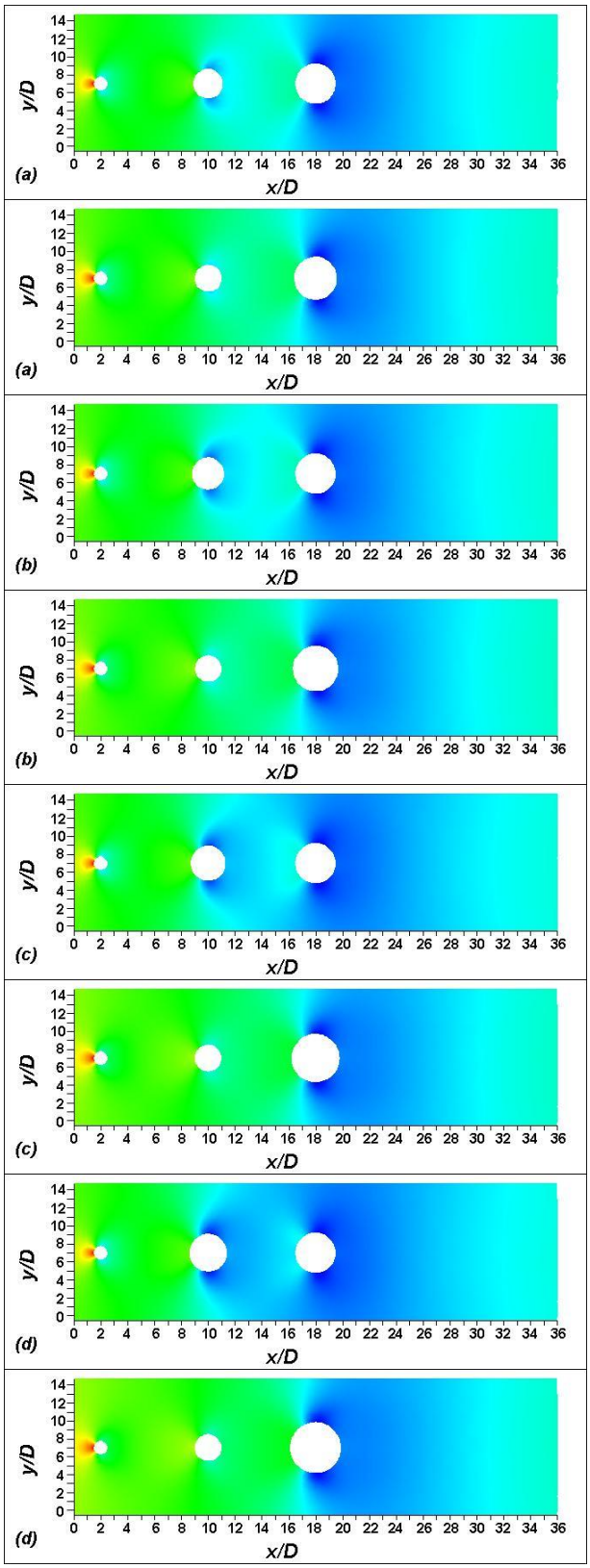
y/D
x/D
(a)
(a)
(b)
(b)
(c)
(c)
(d)
(d)

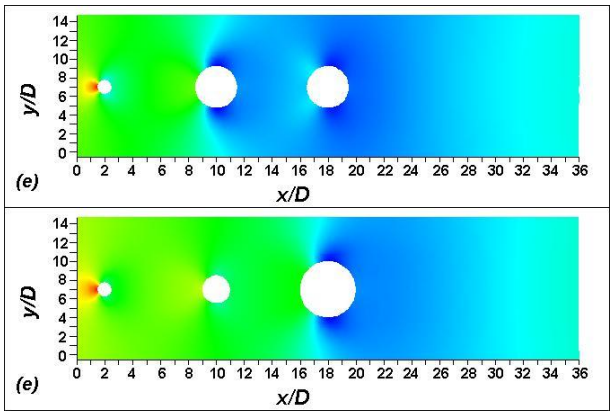

(5) (6)

Figure 10 Pressure Cloud Map

Figure 10 shows a comparison of the superimposed pressure cloud maps for six different sets of parameters, which shows that the pressure field is also symmetrically distributed. The high-pressure area is located in the zone directly in front of the upstream cylinder C_1 wall facing the flow; the low-pressure area is located near the middle and downstream cylinders. As shown in Figs. (1), (2), and (3), when the diameters of the three cylinders are fixed, the low-pressure zone in the flow field shifts to the right as the distance between the cylinders increases, and the position is always at the back side of the cylinder perimeter of the downstream cylinder; for a single cylinder, the pressure at the front side of the cylinder perimeter zone is always greater than that at the backside. When the spacing of the three cylinders is fixed, as shown in Figure (4), if the diameter of C_1 increases, the high-pressure area on its front side expands at the same time. As can be seen in Fig. (5), when the diameter of C_2 increases, two low-pressure areas appear in the flow field, and the low-pressure area around the C_2 cylinder expands outward with the increase of the cylindrical diameter.

2.3 Cylindrical wall drag coefficient

Table 2 Drag coefficient and its change amount (The variable is L_1)

CD Number	C_1	ΔC_d	C_2	ΔC_d	C_3	ΔC_d
1	1.80e-5		1.59e-5		2.78e-5	
2	1.89e-5	9.0e-7	1.64e-5	5.0e-7	2.78e-5	0
3	1.95e-5	6.0e-7	1.74e-5	1.0e-6	2.75e-5	-3.0e-7
4	2.00e-5	5.0e-7	1.87e-5	1.3e-6	2.71e-5	-4.0e-7
5	2.04e-5	4.0e-7	1.99e-5	1.2e-6	2.67e-5	-4.0e-7

As can be seen from Table 2, when the distance L_1 between the upstream cylinder C_1 and the midstream cylinder C_2 increases, the drag coefficient of C_1 increases from 1.80e-5 to 2.04e-5, and the amount of change decreases from 9.0e-7 to 4.0e-7; the drag coefficient of C_2 increases from 1.59e-5 to 1.99e-5, while the number of change increases from 5.0e-7 to 1.2e-6; the drag coefficient of C_3 decreases from 2.78e-5 to 2.67e-5 with a flat change.

Table 3 Drag coefficient and its change amount (The variable is L_2)

CD Number	C_1	ΔC_d	C_2	ΔC_d	C_3	ΔC_d
6	1.88e-5		1.53e-5		2.71e-5	
7	1.89e-5	1.0e-7	1.71e-5	1.8e-6	2.89e-5	1.8e-6
8	1.90e-5	1.0e-7	1.77e-5	6.0e-7	3.01e-5	1.2e-6
9	1.90e-5	0	1.81e-5	4.0e-7	3.16e-5	1.5e-6
10	1.90e-5	0	1.84e-5	3.0e-7	3.30e-5	1.4e-6

As shown in Table 3, when the spacing L_2 between the midstream cylinder C_2 and the downstream cylinder C_3 increases, the drag coefficient of C_1 stays near 1.9e-5; the drag coefficient of C_2 increases from 1.53e-5 to 1.84e-5, and the change decreased from 1.8e-6 to 3.0e-7; the drag coefficient of C_3 increased from 2.71e-5 to 3.30e-5, and the average value of the change was about 1.5e-6.

Table 4 Drag coefficient and its change amount (The variable is $L=L_1=L_2$)

CD Number	C_1	ΔC_d	C_2	ΔC_d	C_3	ΔC_d
11	1.99e-5		1.83e-5		2.85e-5	
12	2.00e-5	1.0e-7	1.99e-5	1.6e-6	2.94e-5	9.0e-7
13	2.04e-5	4.0e-7	2.15e-5	1.6e-6	3.05e-5	1.1e-6
14	2.07e-5	3.0e-7	2.29e-5	1.4e-6	3.16e-5	1.1e-6
15	2.09e-5	2.0e-7	2.41e-5	1.2e-6	3.27e-5	1.1e-6

As shown in Table 4, the drag coefficient of C_1 slowly increases from 1.99e-5 to 2.09e-5 when the spacing (L_1 and L_2) between the upstream cylinder C_1, the midstream cylinder C_2, and the downstream cylinder C_3 increases simultaneously; the drag coefficient of C_2 increased from 1.83e-5 to 2.41e-5, with an average increase of about 1.5e-6; the drag coefficient of C_3 increased from 2.85e-5 to 3.27e-5, with a more uniform change.

Table 5 Drag coefficient and its change amount (The variable is D_1)

CD Number	C_1	ΔC_d	C_2	ΔC_d	C_3	ΔC_d
16	2.37e-5		2.08e-5		3.17e-5	
17	2.71e-5	3.4e-6	1.87e-5	-2.1e-6	3.17e-5	0
18	3.02e-5	3.1e-6	1.66e-5	-2.1e-6	3.17e-5	0
19	3.38e-5	3.6e-6	1.45e-5	-2.1e-6	3.16e-5	-1.0e-7
20	3.76e-5	3.8e-6	1.24e-5	-2.1e-6	3.13e-5	-3.0e-7

As shown in Table 5, when the diameter D_1 of the upstream cylinder C_1 increases, the drag coefficient of C_1 increases significantly from 2.37e-5 to 3.76e-5; the drag coefficient of C_2 decreases flatly from 2.08e-5 to 1.24e-5; and the drag coefficient of C_3 stays around 3.17e-5 with insignificant changes.

Table 6 Drag coefficient and its change amount (The variable is D_2)

CD Number	C_1	ΔC_d	C_2	ΔC_d	C_3	ΔC_d
21	2.06e-5		2.62e-5		2.92e-5	
22	2.06e-5	0	2.99e-5	3.7e-6	2.68e-5	-2.4e-6
23	2.04e-5	-2.0e-7	3.39e-5	4.0e-6	2.41e-5	-2.7e-6
24	2.04e-5	0	3.83e-5	4.3e-6	2.14e-5	-2.7e-6
25	2.03e-5	-1.0e-7	4.32e-5	4.9e-6	1.85e-5	-2.9e-6

As shown in Table 6, when the diameter D_2 of C_2 increases, the drag coefficient of C_1 stays around 2.04e-5 with insignificant changes; the drag coefficient of C_2 increases from 2.62e-5 to 4.32e-5 with a larger magnitude, and the amount of change also increases gradually from 3.7e-6 to 4.9e-6; the drag coefficient of C_3 decreases uniformly from 2.92e-5 to 1.85e-5.

Table 7 Drag coefficient and its change amount (The variable is D_3)

CD Number	C_1	ΔC_d	C_2	ΔC_d	C_3	ΔC_d
26	2.07e-5		2.29e-5		3.63e-5	
27	2.07e-5	0	2.28e-5	-1.0e-7	4.16e-5	5.3e-6
28	2.07e-5	0	2.26e-5	-2.0e-7	4.77e-5	6.1e-6
29	2.07e-5	0	2.25e-5	-1.0e-7	5.45e-5	6.8e-6
30	2.07e-5	0	2.24e-5	-1.0e-7	6.19e-5	7.4e-6

As shown in Table 7, when the diameter D_3 of C_3 increases, the drag coefficient of C_1 stabilizes at 2.07e-5; the drag coefficient of C_2 slowly decreases from 2.29e-5 to 2.24e-5 with insignificant changes; and the drag coefficient of C_3 increases from 3.63e-5 to 6.19e-5 with great magnitude, and the number of change increases from 5.3e-6 to 7.4e-6.

IV. CONCLUSION

As the distance between the cylinders increases, the low-velocity tail flow area of the upstream cylinders is extended and the width decreases along the range until it converges to a point; the drag coefficient of the cylindrical wall at both ends of the distance increases at the same time, and the increase is positively related to the diameter of the cylinders. The increase of upstream cylinder diameter will increase the limit width

and length of its tail flow area. The increase and decrease of the drag coefficient only occur in the upstream cylinder, while the drag coefficient of the wall of the most downstream cylinder increases dramatically with the increase of the cylinder diameter, the change of the drag coefficient of the wall of the upstream and midstream cylinders is extremely weak. In the flow field around the tandem three-cylinder, the maximum value of the vorticity appears on the upstream-most cylinder's on-flow side, near the wall shear layer, and then spreads downstream in a band. The maximum value of pressure is located at the position where the upstream cylinder is facing the incoming flow, and the distribution of the low-pressure area is related to the downstream cylinder diameter.

ACKNOWLEDGEMENTS

The work was supported by the national college students' science and technology innovation project (No. 202211488028).

REFERENCES

[1]. Wang Ying.Research on the Key Characteristics of Spar Vortex-induced Motions[D]. Shanghai Jiao Tong University, 2010.
[2]. Duan Shuangshuai.The Flow Field Characteristics about the Secondary and Primary Cylinders by Numerical Simulation at Low Reynolds Numbers[D]. Dalian University of Technology, 2021.
[3]. Liu Shan, Wang Zhan, Guo Zhen.Numerical Simulation of Flow Field Characteristics Around Offshore Double-Pile Foundation[J]. China Offshore Platform, 2018, 33(06): 37-44.
[4]. Gu Gang.Numerical Simulation of Two-dimensional Flow Around Single & Double Cylinders and Three-Dimensional Oscillation of Heave Plates[D]. Shanghai Jiao Tong University, 2007.
[5]. Du Xiaoqing, Lin Zhiqiang, Wu Gefei.Mode Characteristics and Reconstruction of Flow Field Around Two Tandem Circular Cylinders[J]. Journal of Harbin Institute of Technology, 2022: 1-10.
[6]. Jiang Ke, Zhang Dehua, Qi Yu, Su Yangxuan, Zhao Yi, Tian Runhong.Study on the Characteristics of Flow Around Cylinder at Subcritical Renolds Number[J].Ocean Engineering Equipment and Technology, 2017, 4(01): 37-42.
[7]. Chen Suqin, Gu Ming, Huang Ziping.Numerical Computation of the Flow Around Two Square Cylinders Arranged Side By Side[J]. Applied Mathematics and Mechanics, 2000, 21(2): 131-146.
[8]. Wang X K, Tan S K . Comparison of flow patterns in the near wake of a circular cylinder and a square cylinder placed near a plane wall[J]. Ocean Engineering, 2008, 35(5-6):458-472.
[9]. Tong Xiaojian.Numerical Simulation Research on Flow Characteristics of Flow Around Cylinder under Low Renolds Number Based on Fluent[D]. Yangzhou University, 2021.
[10]. Yin Jianjun.Numerical Investigation of Flow around Cylinders[D].Taiyuan University of Technology, 2021.

Bo-Jie Xu, et. al. "Numerical simulation of flow around three tandem cylinders." *The International Journal of Engineering and Science (IJES)*, 11(9), (2022): pp. 30-49.